THE JOURNAL OF PHYSICAL CHEMISTRY C

ARTICLE

pubs.acs.org/JPCC

Exciton-Related Photoluminescence and Lasing in CdS Nanobelts

B. Liu,[†] R. Chen,[†] X. L. Xu,[†] D. H. Li,[†] Y. Y. Zhao,[†] Z. X. Shen,[†] Q. H. Xiong,[†,‡] and H. D. Sun*[,†]

[†]Division of Physics and Applied Physics, School of Physical and Mathematical Sciences, Nanyang Technological University, Singapore 637371, Singapore

[‡]Division of Microelectronics, School of Electrical and Electronics Engineering, Nanyang Technological University, Singapore 639798, Singapore

ABSTRACT: We present exciton-related optical studies of cadmium sulfide (CdS) nanobelts. Photoluminescence (PL) properties of CdS nanobelts are analyzed by using high spectral resolution spectroscopy from 10 to 300 K. The PL spectrum at 10 K shows rich spectral features which are identified, by means of temperature-dependent spectral evolution, to be the recombinations of free excitons, excitons bound to neutral impurities, and donor−acceptor pairs. The strong excitonic emission in our samples enables the observation of random lasing action at room temperature with a lasing threshold pump density of ~0.1402 ± 0.0060 MWcm^{-2}. Notably, temperature-dependent pump thresholds exhibit a characteristic temperature as high as 195.3 ± 12.7 K, implying a good thermal stability of the lasing behavior and potential high temperature operation. Our studies not only elucidate the intrinsic physical properties of our high quality nanomaterial but also reveal the promising applications in photonics.

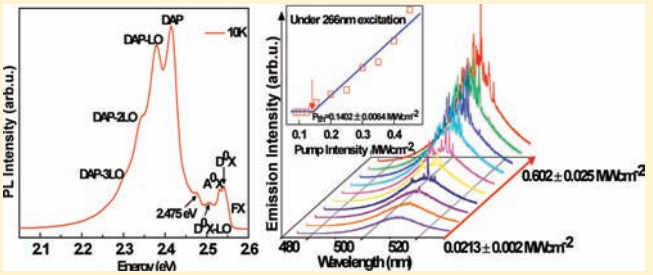

INTRODUCTION

As an important II−VI semiconductor material, CdS has a direct band gap of 2.45 eV[1] at room temperature and thus is deemed to be a possible candidate for optoelectronic applications in the visible spectrum range. Previously CdS-based materials have not received much attention as other II−VI materials, like ZnSe[2,3] and ZnO,[4−6] partially due to the unavailability of suitable substrates for high quality epitaxial growth. Such a picture has been totally changed in recent years with the advances in the fabrication of low dimensional semiconductor nanostructures which lead to various optical devices (lasers,[7] detectors,[8] waveguides,[9] etc.) at nanoscale for future integrated photonics. A variety of techniques have been employed to fabricate various CdS nanostructures such as ion implantation,[10] vapor−solid,[11] and electrochemical[12] growth method, etc. Meanwhile, photonic devices based on CdS nanostructures, especially nanolasers, have achieved remarkable success, represented by the early demonstration of CdS nanowire lasers[13] and recent realization of CdS square subdiffraction limited plasmonic laser.[14] In developing semicomductor-based lasers, an important concern is the thermal stability of the pumping threshold specified by the so-called characteristic temperature. So far there has been no effort paid to this issue for CdS-based nanolasers. Moreover, the detailed optical investigation on CdS nanomaterials regarding the light emission mechanisms is still highly demanded, especially the exciton-related emission has not been firmly identified due to the low crystal quality of sample.

In this work, the optical properties of high quality CdS nanobelts were studied through temperature dependent experiments. The band-edge recombination in visible region can be assigned as free exciton (FX), exciton bound to neutral donor (D^0X) impurities, exciton bound to neutral acceptor (A^0X) impurities, and donor−acceptor pairs (DAP) by systematic analysis. Such rich and clear PL spectral structures and the presence of FX should be attributed to the high crystal quality and band-edge emission efficiency of our CdS nanobelts, supported by the absence of deep level related emission. The efficient excitonic emission allows for the observation of lasing under the excitation of a 266 nm pulsed laser, and the sample exhibits strong random lasing action at room temperature with a pumping threshold of 0.1402 ± 0.0064 MWcm^{-2}. The temperature-dependent pumping threshold for lasing is systematically measured from 10 to 300 K, from which the characteristic temperature is determined to be as high as 195.3 ± 12.7 K. Our careful analyzing the temperature-dependent PL spectra gives us a clear picture about exciton behavior from low temperature to room temperature. We recognize that the electrical and optical driven lasers could have different behaviors, but the fundamental optical properties especially the radiative recombination mechanisms should be the same. In addition, temperature-dependent pumping threshold is directly related to the stability of laser operation. Therefore, our detailed optical study is important for material selection and fabrication.

EXPERIMENTAL SECTION

Our samples were synthesized using a home-built vapor transport chemical vapor deposition system. In general, CdS powder (99.995%) from Sigma-Aldrich was used as a source material contained in a quartz boat, which was put into the center of the quartz tube. A silicon substrate was then put into the downstream. The tube was purged with Ar/5% H_2 to evacuate

Received: April 16, 2011
Revised: June 1, 2011
Published: June 01, 2011

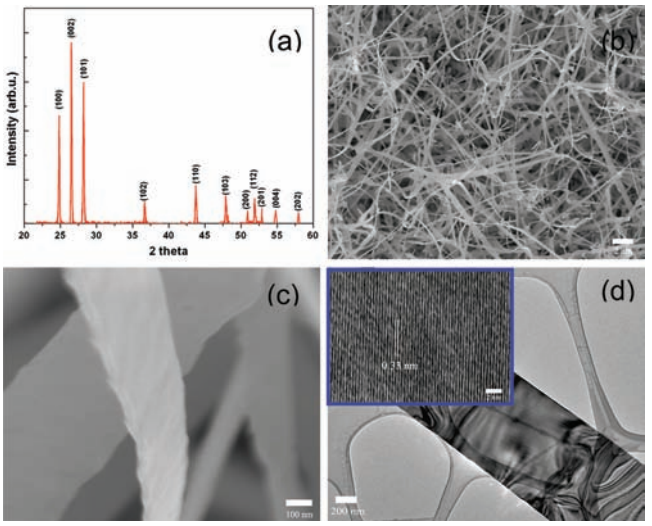

Figure 1. (a) XRD pattern of the as-synthesized CdS nanobelts. (b) Low and (c) High resolution SEM images of CdS nanobelts deposited on Si substrate. (d) TEM and HRTEM (inset) image of CdS nanobelt.

first and then the furnace was heated up to 670 °C with the carrying gas Ar with a flow rate of 50 sccm for half an hour.

The crystalline structure was characterized by X-ray diffraction (XRD, with Cu K_α = 0.15419 nm; Bruker D8 Advance diffractometer), field emission scanning electron microscope (FESEM, JEOL JSM-6700F), transmission electron microscopy (TEM, JEM-200CX), and high resolution transmission electron microscopy (HRTEM, JEOL-2010F). For temperature-dependent PL measurement, the 325 nm line from a He−Cd laser was used as the excitation source. The PL signal was collected in a backscattering geometry and detected by a photomultiplier tube using the standard lock-in technique. A close-cycled helium cryostat (Advanced Research System) was used to provide continuous temperature variation from 10 K to room temperature. For random lasing measurement, a pulsed Nd:YAG fourth harmonic (266 nm) laser was used, and the signal was detected by a UV-enhanced charged coupled device (CCD). The pulse width and repetition rate of the laser are about 1 ns and 60 Hz, respectively.

RESULTS AND DISCUSSION

Figure 1a shows the XRD pattern of the CdS nanobelts, and all the diffraction peaks can match very well with a wurtzite (hexagonal) structure of CdS crystal. Figures 1b,c are the low and high magnification SEM images. From Figure 1b we can see that a large amount of CdS nanobelts are distributed randomly on the substrate. The typical length of nanobelts is about tens to hundred micrometers, and the thickness is on the scale of tens of nanometers, while the width is on the scale of tens of nanometers to micrometers. In addition to the large variation in size distribution, there is also some roughness along the belts. The detailed microstructure information is further studied by TEM. Figure 1d is a representative TEM image of the nanobelt which reveals that the nanobelt is relatively uniform. A HRTEM is shown in the inset of Figure 1d, which reveals the CdS nanobelts are single crystal. The measured lattice spacing is ~0.33 nm, which corresponds to the {002} lattice plane of hexagonal CdS.

The typical PL spectrum measured at 10 K is shown in Figure 2. The CdS nanobelts show a very strong near band emission, and no obvious surface states related emission[15] is

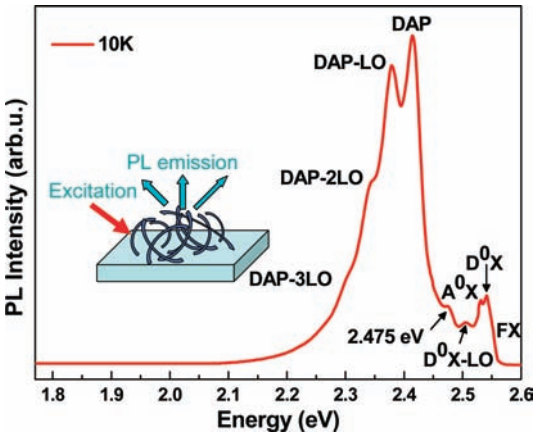

Figure 2. PL spectrum of CdS nanobelts taken at 10 K. The inset is excitation and PL emission configuration.

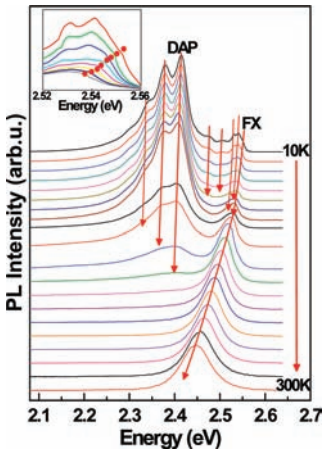

Figure 3. Temperature-dependent PL spectra of the CdS nanobelts in the range from 10 to 300 K. Dashed lines show the peak evolution. The enlarge figure of the higher energy part is shown in the inset, and the FX is indicated by the solid red points.

found in lower energy region around 1.8 eV, indicating the high crystal quality of our sample. From the figure we can see that the 10 K spectrum consists of nine distinct peaks at ~2.552, 2.540, 2.531, 2.505, 2.475, 2.414, 2.378, 2.340, and 2.302 eV. The high crystal quality and high spectral resolution (~0.8 meV) of the measurement should be responsible for our rich observation. Some of the peaks can be reasonably assigned by their characteristic energy and systematic analysis. Because of the crystal field and spin−orbit interaction, the valence band of CdS will be split into three ones with which an electron may bind to form three different excitons named A, B, and C. The emission band at 2.552 eV, very close to the energy of A exciton in wurtzite CdS structure,[16] is assigned to FX emission, which can be elucidated by carefully analyzing temperature-dependent PL spectra as shown below. The peaks located at 2.540 and 2.531 eV have also been found in another reference[17] and can be assigned as D^0X and A^0X, respectively. Considering the energy of the longitudinal optical (LO) phonon of CdS is about 38 meV,[15] the next peak on the lower energy side of A^0X can be reasonably attributed to the first LO phonon replica of D^0X.[18] From the temperature-dependent PL spectra, we can see that the peak located at 2.475 eV almost does not change with increasing

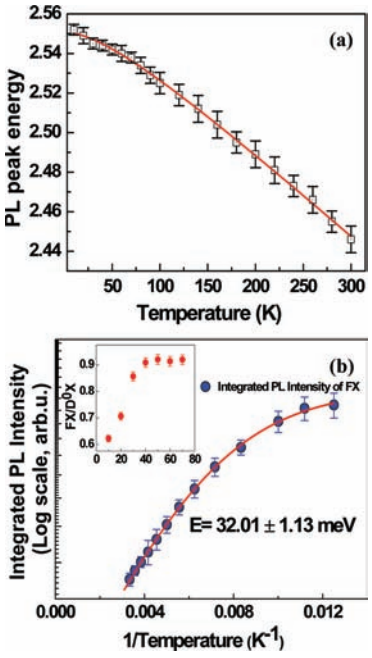

Figure 4. (a) Temperature-dependent red-shift of FX, and the solid red curve is the corresponding fit based on Varshni equation. The error bar is enlarged 3 times for clarification. (b) Natural logarithm of the integrated PL intensity of FX as a function of $1/T$, and the red curve is the corresponding fit based on Arrhenius equation. The error bar is enlarged 8 times for clarification. The inset is the ratio of FX to D^0X peak intensities as a function of temperature. The error bar is enlarged 2 times for clarification.

temperature and disappears around 40 K. The original of this peak is not clear at this stage. The peak at 2.414 eV is assigned to DAP, which is widely found in other wide band II−VI group semiconductor materials, and one of the obvious characteristics of DAP is the LO phonons will appear at lower energy side. The energy spacing among peaks at 2.414, 2.378, 2.340, and 2.304 eV is around 38 meV, so they are assigned as higher-order LO phonon replicas of DAP.

Figure 3 is the temperature-dependent PL spectra taken from 10 to 300 K. With temperature increasing, the intensity of PL emission decreased at elevated temperatures. The peak intensity of A^0X faded and became irresolvable around 80 K and then merged with the peak of FX. Comparing to DAP, the PL intensity of D^0X decreased faster before 70 K because of the smaller ionizing energy of D^0X. When the temperature increased, the D^0X will be thermally ionized and finally turn into FX. The FX becomes more and more prominent when temperature goes up until room temperature. This phenomenon is well-known in wide-band-gap semiconductors. A close look at the trend of the DAP emission band indicated that the relative intensity of DAP decreased slowly before 90 K and reduced very quickly when the temperature increased. The DAP peak almost disappeared at 140 K, and the LO phonon replicas of DAP became unresolved when the temperature reached 120 K. This phenomenon reveals that the impurities involved in DAP recombination process need larger energy to ionize them comparing with the ionizing energy of D^0X. The magnified figure of the higher energy part is shown in the inset of Figure 3 where the FX transitions at various temperatures are denoted by solid points.

The temperature-dependent red shift of FX peak energy is shown in Figure 4a. Assuming the exciton binding energy does not change with temperature, increased electron phonon interaction and the lattice expansion with increasing temperature should be responsible for the red-shift of excitonic emission line.[19,20] The electron phonon interaction effect can cause the shift of the conduction band and valence band which will result in a quadratic variation of the energy gap at low temperature and a linear shift at high temperature. The fundamental band gap as a function of temperature can be well fitted with empirical equation describing the semiconductor band gap temperature evolution, viz. Varshni equation

$$E(T) = E(0) - \frac{\alpha T^2}{T+\beta} \quad (1)$$

where $E(0)$ is the band gap at 0 K; α and β are constants related to materials which are deemed as Varshni's coefficients. Especially, α stands for the linear shift of $E(T)$ at high temperature and β represents the quadratic variation of $E(T)$ at low temperature. The exciton binding energy of CdS is about 28 meV,[21] so excitons can exist even at room temperature; thus, we can fit the PL peak energy from 10 to 300 K excluding the effect of the free carrier recombination. As shown in Figure 4a, the Varshni fitting curve (solid red line) fits our experimental result very well. The fit yields $E(0) = 2.5511 \pm 0.0007$ eV, $\alpha = 0.43 \pm 0.01$ meV K^{-1}, and $\beta = 78.280 \pm 11.299$ K. The fitting results are very similar to previous results.[16] Differentiating the Varshni equation with respect to temperature, we obtain

$$\frac{dE(T)}{dT} = -\alpha\left[\frac{2T}{T+\beta} - \frac{T^2}{(T+\beta)^2}\right] \quad (2)$$

and the temperature coefficient $dE(T)/dT$ for CdS at 300 K can be determined to be -0.411 ± 0.013 meV K^{-1}. This value is in good agreement with the literature[16,22] and supports our assignment.

Figure 4b shows the variations in integrated PL intensity of FX as a function of $1/T$ between 80 and 300 K. Then integrated PL intensity can be well reproduced by the Arrhenius[23] equation

$$I = I_0/[1 + c\exp(-E_a/k_B T)] \quad (3)$$

where E_a is the activation energy for thermal activation process, k_B is Boltzmann constant, and c is the relative ratio of nonradiative recombination. From the fitting we can get the activation energy for thermal activation process is 32.01 ± 1.13 meV, which is comparable with the thermal energy required for dissociation the free exciton of CdS (28 meV).[21] The fitting results support our assignment of FX. The inset of Figure 4b shows the ratio of FX to D^0X peak intensities as a function of temperature, and we can see the ratio increases with increasing temperature. The D^0X will get thermal energy with increasing temperature, and when the thermal energy is close to the activation energy of D^0X exciton will separate from the donor impurity and dissociate into a free exciton and a neutral donor, so the peak intensity ratio between FX and D^0X will increase. This peak intensity ratio trend also supports our assignment of FX and D^0X.

Figure 5a shows the PL spectra of CdS nanobelts pumped by a 266 nm pulsed laser at room temperature. Before the pump density reached P_{th}, where P_{th} stands for the pump threshold, we can only see a broad spontaneous emission with full width at half-maximum (FWHM) about 15.14 ± 0.07 nm. When the pump density reached P_{th}, some sharp peaks with line width as narrow as 0.31 ± 0.02 nm appear from the broad spontaneous emission spectrum, which is about 50 times narrower than that of the spontaneous emission band, indicating the occurrence of lasing

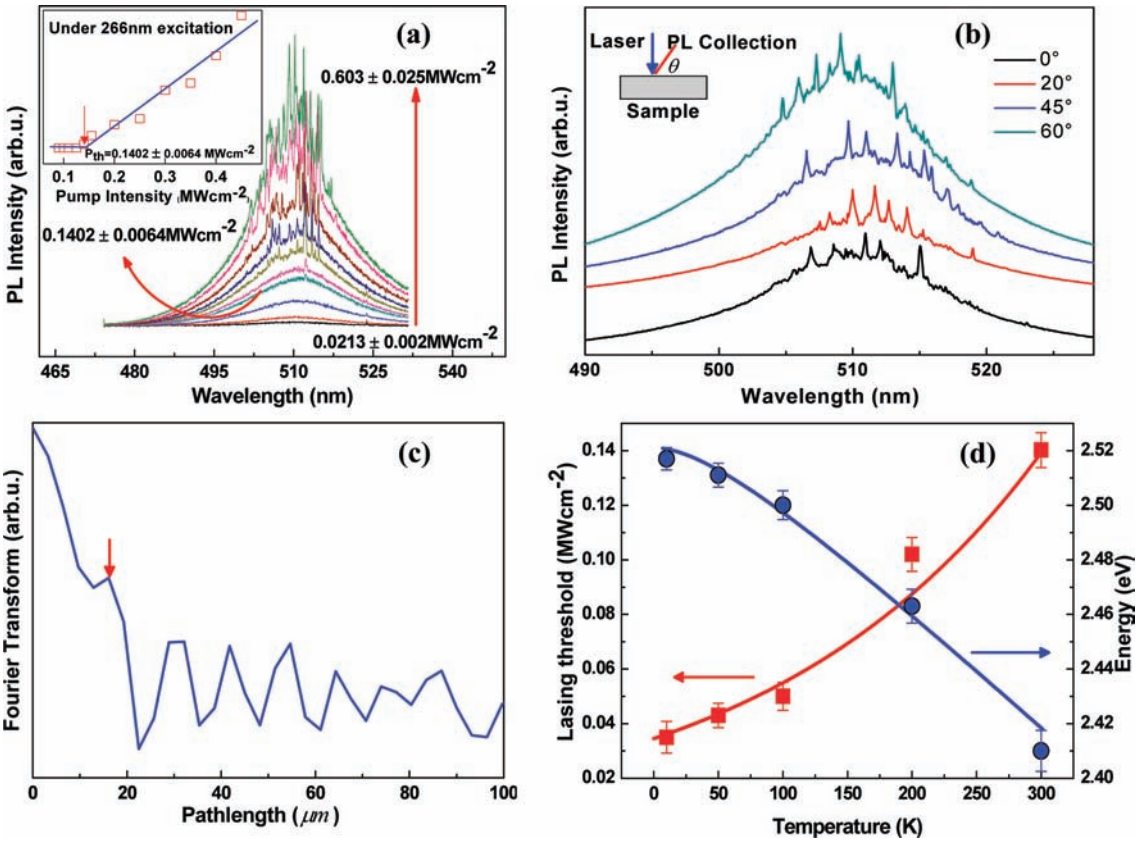

Figure 5. (a) Lasing spectra and integrated emission intensity as a function of optical pump density (inset) of random assembly CdS nanobelts at room temperature. (b) Emission spectra of CdS nanobelts observed at different angles. (c) Fourier transform of the lasing spectrum with pump power of 0.571 MWcm^{-2}. (d) Plots of lasing emission envelop energy and P_{th} vs temperature. The blue solid line is Varshni fitting curve (shift down for clarification). The red solid line is the fitting curve of the experimental data.

action. With the pump density increasing, more and more lasing modes were emerged. A plausible explanation may relate the lasing to Fabry−Pérot cavity, formed by the two end facets of single nanobelts. However, the characteristics of the longitudinal lasing modes do not support this interpretation but can be attributed to random lasing. In randomly oriented nanobelts, the emitted light will experience strong scattering and can come back to its original scatter, therefore forming the close-loop path. And there are many this kind of paths in the sample serving as round-trip cavity for the emitted light. In all the loops, the probability of the light returning to its original scatter is dissimilar, which means that the optical losses of these cavities are different. When laser power pumped on the nanobelts increases, the optical gain will surpass the optical loss in the round-trip cavities and laser will be generated and oscillate in these cavities. The lasing frequencies (longitudinal modes) are governed by the cavity length. The discrete narrow peaks raised from the lasing process will appear on the broad spontaneous emission spectra. Further increasing the pump power, there will be more and more discrete peaks shown on the emission spectra because more loops meet the threshold requirement.[24] Our experimental results clearly indicate that the coherent random lasing action occurs in our sample. The inset of Figure 5a is the integrated emission intensity as a function of optical pump density, which shows an obvious threshold around 0.1402 ± 0.0064 MWcm^{-2}, an indicator of lasing action. In order to further proving random lasing action, the lasing spectra measured at different angles are shown in Figure 5b. Different angles give dissimilar lasing spectra due to different laser cavities formed by multiple scattering, which is typical for random lasing action.[25,26]

To determine the laser cavity length of the closed-loop random lasing of CdS nanoblets, the Fourier transform (FT)[27,28] of the lasing spectrum is shown in Figure 5c. The FT of the lasing spectrum will result in a spectrum containing the fundamental optical path related to the cavity length. If the unit of lasing spectrum is in wavenumber, the unit of FT spectrum will be in length. The random lasing spectrum with power density 0.571 ± 0.023 MWcm^{-2} was chosen as FT-treated spectrum. In the FT spectrum, the cavity length L can be determined by the following equation

$$L = \frac{2d\pi}{n} \tag{4}$$

where d is optical path length at which the peak is obvious at FT spectrum and n is the refractive index of the gain medium. From the figure we found an obvious peak at 16.02 ± 0.12 μm and a series of peaks that appear at 32.04 ± 0.08, 41.03 ± 0.09, and 64.06 ± 0.13 μm. The peak at ∼16 μm should be attributed to light passing through multiple trips of the optical path. So the fundamental cavity length is determined to be 40.2 ± 0.3 μm, which is obtained from the d (16.02 ± 0.12 μm) and n (2.5 for CdS). This calculated cavity length is much smaller than the pump spot size focused on the sample which has the diameter in the millimeter range.

The peak energy of lasing emission envelope and P_{th} versus temperature are plotted in Figure 5d. The evolvement of peak energy of the emission envelop is similar to FX. The evolvement trend follows the Varshni fitting curve (blue solid line which is shifted down for clarification) of FX very well. This indicates that the lasing mechanism is closely related to radiative recombination of free excitons. The slight energy difference between the lasing emission envelope and FX can be attributed to thermal effect caused by the pulse laser.

It is found that the P_{th} increases exponentially with temperature and can be fitted by the empirical formula

$$P_{th}(T) = P_0 \exp(T/T_c) \quad (5)$$

where P_0 represents the threshold pump intensity at $T = 0$ K and T_c is the characteristic temperature reflecting the temperature stability of a laser.[29] The high value of T_c stands for better high temperature laser performance. From the fitting, it is found that the T_c of our CdS nanobelt laser is 195.3 ± 12.7 K. Comparing with previously reported ZnO nanoneedles,[30] the T_c of our sample is higher. In principle, the increased pumping threshold at elevated temperatures for a semiconductor laser originates from the increased nonradiative recombination. The characteristic temperature T_c is closely related to the electronic structures as well as the number and distribution of nonradiative centers in the devices. As investigated by temperature dependent PL, our sample is dominated by strong excitonic signature in all radiative recombinations. The absence of deep level optical transition and the existence of free excitons at low temperature are strong evidence of low defect density. Moreover, recombination of stable excitons is advantageous over electron−hole pair recombination in narrower spectral gain and reduced Auger recombination. The relatively high T_c of our sample not only reveals high crystal quality of CdS nanobelts but also demonstrates the potential of CdS as a laser material for better temperature stability and higher temperature operation.

CONCLUSIONS

In conclusion, high quality CdS nanobelts were fabricated by chemical vapor deposition (CVD) process and characterized by XRD, SEM, and TEM. The PL spectrum of CdS nanobelts at 10 K shows very rich spectral features which are identified to be FX, D^0X, and DAP by carefully analyzing temperature-dependent PL spectra. The fit results based on Varshni empirical equations support our assignment of FX. The thermal activation energy of FX is estimated to be 32.01 ± 1.13 meV. Upon the excitation of a 266 nm pulse laser, the sample exhibits random lasing action with excitonic properties, and the lasing threshold is 0.1402 ± 0.0060 MWcm^{-2} at room temperature. The temperature-dependent pumping threshold reveals a characteristic temperature as high as 195.3 ± 12.7 K. Our studies not only elucidate the intrinsic physical properties of this novel nanomaterial but also reveal the possible application in photonics.

AUTHOR INFORMATION

Corresponding Author

*E-mail: hdsun@ntu.edu.sg.

REFERENCES

(1) Wang, S. *Fundamentals of Semiconductor Theory and Device Physics*; Prentice-Hall: New York, 1989.

(2) Steven, C. E.; Zu, L. J.; Michael, I. H.; Alexander, L. E.; Thomas, A. K.; David, J. N. *Nature* **2005**, *436*, 91.

(3) Norris, D. J.; Yao, N.; Charnock, F. T.; Kennedy, T. A. *Nano Lett.* **2001**, *1*, 3.

(4) Zhang, B. P.; Segawa, Y.; Wakatsuki, K.; Kashiwaba, Y.; Haga, K. *Appl. Phys. Lett.* **2001**, *79*, 3953. Sun, H. D.; Makino, T.; Segawa, Y.; Kawasaki, M.; Ohtomo, A.; Tamura, K.; Koinuma, H. *Appl. Phys. Lett.* **2001**, *78*, 3385.

(5) Ashrafi, A. B. M. A.; Binh, N. T.; Zhang, B. P.; Segawa, Y. *Appl. Phys. Lett.* **2004**, *84*, 2814.

(6) Zeng, H. B.; Duan, G. T.; Li, Y.; Yang, S. K.; Xu, X. X.; Cai, W. P. *Adv. Funct. Mater.* **2009**, *19*, 1.

(7) Cao, B. L.; Jiang, Y.; Wang, C.; Wang, W. H.; Wang, L. Z.; Niu, M.; Zhang, W. J.; Li, Y. Q.; Lee, S. T. *Adv. Funct. Mater.* **2007**, *17*, 1501.

(8) Gu, Y.; Kwak, E. S.; Lensch, J. L.; Allen, J. E.; Odom, T. W.; Lauhon, L. J. *Appl. Phys. Lett.* **2005**, *87*, 043111.

(9) Barrelet, C. J.; Greytak, A. B.; Lieber, C. M. *Nano Lett.* **2004**, *4*, 1981.

(10) Kanemitsu, Y.; Inagaki, T. J.; Ando, M.; Matsuda, K.; Saiki, T.; White, C. W. *Appl. Phys. Lett.* **2002**, *81*, 141.

(11) Xu, L.; Su, Y.; Cai, D.; Chen, Y. Q.; Feng, Y. *Mater. Lett.* **2006**, *60*, 1420.

(12) Routkevitch, D.; Bigioni, T.; Moskovits, M.; Xu, J. M. *J. Phys. Chem.* **1996**, *100*, 14037.

(13) Duan, X. F.; Huang, Y.; Agarwal, R.; Lieber, C. M. *Nature* **2003**, *421*, 241.

(14) Ma, R. M.; Oultom, R. F.; Sorger, V. J.; Bartal, G.; Zhang, X. *Nature Mater.* **2011**, *10*, 110.

(15) Liu, W. F.; Jia, C.; Jin, C. G.; Yao, L. Z.; Cai, W. L.; Li, X. G. J. *Cryst. Growth* **2004**, *269*, 304.

(16) Imada, A.; Ozaki, S.; Adachi, S. J. *Appl. Phys.* **2002**, *92*, 1793.

(17) Thomas, D. G.; Hopfield, J. J. *Phys. Rev.* **1962**, *128*, 2135.

(18) Chen, C. H.; Chen, Y. F.; Shih, A.; Lee, S. C.; Jiang, H. X. *Appl. Phys. Lett.* **2001**, *78*, 3035.

(19) Varshni, Y. P. *Physica* **1967**, *34*, 149.

(20) Liu, B.; Cheng, C. W.; Chen, R.; Shen, Z. X.; Fan, H. J.; Sun, H. D. *J. Phys. Chem. C* **2010**, *114*, 3407.

(21) Ip, K. M.; Wang, C. R.; Li, Q.; Hark, S. K. *Appl. Phys. Lett.* **2004**, *84*, 795.

(22) Gutsche, E.; Voigt, J. In *II-VI Semiconducting Compounds*; Thomas, D. G., Ed.; Benjamin: New York, 1967.

(23) Gu, X.; Huo, K.; Qian, G.; Fu, J.; Chu, P. K. *Appl. Phys. Lett.* **2008**, *93*, 203117.

(24) Cao, H.; Zhao, Y. G.; Ong, H. C.; Ho, S. T.; Dai, J. Y.; Wu, J. Y.; Chang, R. P. H. *Appl. Phys. Lett.* **1998**, *73*, 3656.

(25) Cao, H.; Zhao, Y. G. *Phys. Rev. Lett.* **1999**, *82*, 2278.

(26) Chen, R.; Utama, M. I. B.; Peng, Z. P.; Peng, B.; Xiong, Q. H.; Sun, H. D. *Adv. Mater.* **2011**, *23*, 1404.

(27) Polson, R. C.; Chipouline, A.; Vardeny, Z. V. *Adv. Mater.* **2001**, *13*, 760.

(28) Polson, R. C.; Levina, G.; Vardeny, Z. V. *Appl. Phys. Lett.* **2000**, *76*, 3858.

(29) Yang, H. Y.; Yu, S. F.; Li, G. P.; Wu, T. *Opt. Express* **2010**, *18*, 13647.

(30) Yang, H. Y.; Lau, S. P.; Yu, S. F.; Abiyasa, A. P.; Tanemura, M.; Okita, T.; Hatano, H. *Appl. Phys. Lett.* **2006**, *89*, 011103.